

A Direct Model Predictive Control Strategy with Optimized Sampling Interval

Qifan Yang, *Student Member, IEEE*, Petros Karamanakos, *Senior Member, IEEE*,
Tobias Geyer, *Senior Member, IEEE*, and Ralph Kennel, *Senior Member, IEEE*

Abstract—In this paper we present a direct model predictive control (MPC) scheme with time-varying sampling intervals. These sampling intervals are computed based on modulation (half-)cycles, which are obtained offline and stored in a look-up table. By utilizing the optimized modulation (half-)cycles and combining control and modulation in one computational stage, the proposed direct MPC scheme achieves lower current total harmonic distortion (THD) than conventional linear controllers with a dedicated modulator, and fast transient responses that characterize direct control methods. The effectiveness of the proposed control scheme is verified on a variable speed drive system consisting of a two-level voltage source inverter and an induction machine.

I. INTRODUCTION

Model predictive control (MPC) is a time-domain control strategy that has received increasing interest from the power electronics community in the recent years [1], [2]. Unlike the conventional controllers that are designed in the frequency domain, MPC formulates the control problem as a (constrained) optimization problem. By doing so, the nonlinearities and physical constraints of the system can be included in a straightforward manner [3].

MPC of power electronic systems can be formulated either as direct MPC, i.e., a controller without a dedicated modulation stage, or as indirect MPC, where a modulator is used to translate the controller commands into switching signals [2]. The former, however, particularly in its form as direct MPC with output reference tracking—commonly referred to as finite control set MPC (FCS-MPC)—can lead to significant current distortions, especially when poorly designed [4]. As a result, it cannot outperform the steady-state performance of conventional modulator-based techniques, such as field oriented control (FOC) with space vector modulation (SVM) [5].

To address this issue of direct MPC strategies, there have been some MPC-based schemes that emulate the behavior of a modulator by introducing additional switching events within the sampling interval [6]–[12]. Specifically, these schemes ensure that all phases of the power converter switch within the sampling interval, thus resulting in a fixed switching frequency, even though a modulator is not employed. In doing

so, a behavior on par with that of conventional pulse width modulation (PWM) strategies, such as SVM, can be achieved.

Nevertheless, as is the case with conventional PWM strategies, these methods use a fixed sampling interval—which in essence is the modulation (half-)cycle—and vary the duty cycle of the converter switches to achieve a desired average output voltage which will lead to the desired reference tracking. As a result, the harmonics generated due to the switching nature of the converters can still be relatively high. The work in [13] showed that by using time-varying sampling intervals and considering them as optimization variables the harmonic distortion caused by the modulator can be further reduced. However, a non-fixed sampling interval poses big challenges for closed-loop control, especially when proportional-integral (PI) controllers are considered. Therefore, the so-called optimized modulation half-cycles were implemented only in an open-loop fashion in [13].

To exploit the advantages associated with optimized time-varying sampling intervals, a direct MPC strategy is proposed in this paper. Specifically, the developed MPC scheme tackles the control and modulation in one constrained optimization problem, akin to [10] and [12]. The optimization problem underlying direct MPC computes the time instants within the optimized time-varying sampling intervals where all three phases of the converter need to switch in a consecutive manner such that accurate output reference tracking is ensured with as little distortions as possible. In doing so, superior steady-state performance as well as fast dynamic responses during transients can be achieved. To demonstrate this, a low-voltage drive system, consisting of a two-level inverter and an induction machine, serves as a case study.

II. MATHEMATICAL MODEL OF THE SYSTEM

The examined system consists of a three-phase two-level voltage source inverter and an induction machine (IM), as shown in Fig. 1. The dc-link voltage is assumed to be constant and equal to its nominal value V_{dc} . The modelling of the system as well as the formulation of the control problem are done in the stationary orthogonal $\alpha\beta$ reference frame. Therefore, any variable $\xi_{abc} = [\xi_a \ \xi_b \ \xi_c]^T$ in the abc -plane is transformed into a variable $\xi_{\alpha\beta} = [\xi_\alpha \ \xi_\beta]^T$ in the $\alpha\beta$ -plane via the Clarke transformation matrix \mathbf{K} .¹

Consider the three-phase switch position of the two-level inverter $\mathbf{u}_{abc} = [u_a \ u_b \ u_c]^T$, where $u_x \in \mathcal{U} = \{-1, 1\}$, with

¹In the sequel of the paper, the subscript $\alpha\beta$ used to denote variables in the $\alpha\beta$ -plane is omitted to simplify the notation.

Q. Yang and R. Kennel are with the Chair of Electrical Drive Systems and Power Electronics, Technische Universität München, Munich 80333, Germany; e-mail: qifan.yang@tum.de, ralph.kennel@tum.de

P. Karamanakos is with the Faculty of Information Technology and Communication Sciences, Tampere University, 33101 Tampere, Finland; e-mail: p.karamanakos@ieee.org

T. Geyer is with ABB System Drives, 5300 Turgi, Switzerland; e-mail: t.geyer@ieee.org

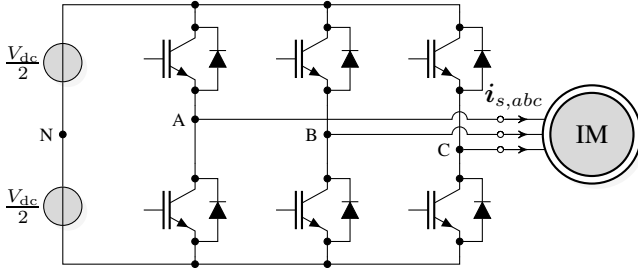


Fig. 1: Two-level three-phase voltage source inverter driving an IM.

$x \in \{a, b, c\}$, is the single-phase switch position. The voltage applied to the machine terminals is calculated as

$$\mathbf{v}_s = \frac{V_{dc}}{2} \mathbf{u} = \frac{V_{dc}}{2} \mathbf{K} \mathbf{u}_{abc}. \quad (1)$$

The dynamics of the squirrel-cage IM can be described by the following differential equations [14]

$$\frac{d\mathbf{i}_s}{dt} = -\frac{1}{\tau_s} \mathbf{i}_s + \left(\frac{1}{\tau_r} \mathbf{I}_2 - \omega_r \begin{bmatrix} 0 & -1 \\ 1 & 0 \end{bmatrix} \right) \frac{X_m}{D} \boldsymbol{\psi}_r + \frac{X_r}{D} \mathbf{v}_s \quad (2a)$$

$$\frac{d\boldsymbol{\psi}_r}{dt} = \frac{X_m}{\tau_r} \mathbf{i}_s - \frac{1}{\tau_r} \boldsymbol{\psi}_r + \omega_r \begin{bmatrix} 0 & -1 \\ 1 & 0 \end{bmatrix} \boldsymbol{\psi}_r, \quad (2b)$$

where R_s (R_r) is the stator (rotor) resistance, X_{ls} (X_{rs}) the stator (rotor) leakage reactance, and X_m the mutual reactance. Moreover, $\tau_s = X_r D / (R_s X_r^2 + R_r X_m^2)$ and $\tau_r = X_r / R_r$ are the transient stator and rotor time constants, respectively, where the constant D is defined as $D = X_s X_r - X_m^2$, with $X_s = X_{ls} + X_m$ and $X_r = X_{lr} + X_m$.

Based on (2), the model of the drive system in continuous-time state-space representation is written as

$$\frac{d\mathbf{x}(t)}{dt} = \mathbf{F} \mathbf{x}(t) + \mathbf{G} \mathbf{K} \mathbf{u}_{abc}(t) \quad (3a)$$

$$\mathbf{y}(t) = \mathbf{C} \mathbf{x}(t), \quad (3b)$$

where the state vector is $\mathbf{x} = [i_{s\alpha} \ i_{s\beta} \ \psi_{r\alpha} \ \psi_{r\beta}]^T$, while the three-phase switch position and the stator current are the system input and output, respectively, i.e., $\mathbf{u}_{abc} = [u_a \ u_b \ u_c]^T$ and $\mathbf{y} = [i_{s\alpha} \ i_{s\beta}]^T$. Moreover, matrices \mathbf{F} , \mathbf{G} , and \mathbf{C} are the system, input and output matrices, respectively, and they can be easily derived from (2).

Finally, with the help of forward Euler discretization the discrete-time state-space model of the system becomes

$$\mathbf{x}(k+1) = \mathbf{A} \mathbf{x}(k) + \mathbf{B} \mathbf{K} \mathbf{u}_{abc}(k) \quad (4a)$$

$$\mathbf{y}(k) = \mathbf{C} \mathbf{x}(k), \quad (4b)$$

with $k \in \mathbb{N}$, $\mathbf{A} = \mathbf{I} + \mathbf{F} T_s$, and $\mathbf{B} = \mathbf{G} T_s$, where \mathbf{I} is the identity matrix of appropriate dimensions, and T_s the sampling interval. Note, however, that, as shown in the sequel, the system eventually is not discretized based on T_s , but rather by using the appropriate optimized sampling interval T_k , as computed in Section III-A.

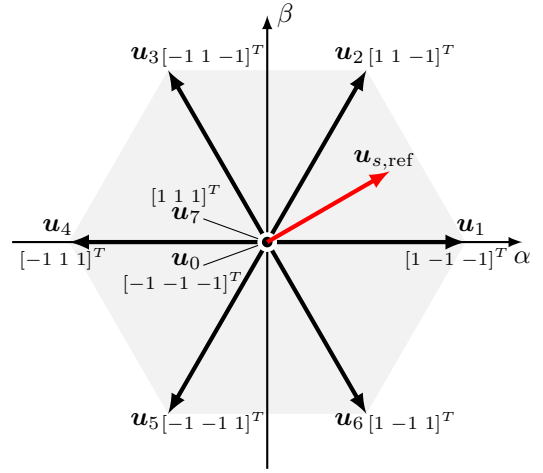


Fig. 2: Two-level inverter switch positions in the stationary ($\alpha\beta$) plane.

III. DIRECT MPC WITH OPTIMIZED SAMPLING INTERVAL

A direct MPC scheme that allows the converter switches to switch not only at the discrete time steps, but also at any time instant within the sampling interval, was initially proposed in [10]. Moreover, by forcing each phase to switch once per sampling interval T_s , a switching pattern similar to SVM is achieved. By doing so, the direct MPC scheme achieves similar steady-state behavior as conventional FOC with SVM. However, the total harmonic distortion (THD) of the stator current can be further decreased by considering the sampling interval, namely the equivalent modulation half-cycle, as an optimization variable [13]. Based on the above, in this work, the aforementioned direct MPC scheme is combined with optimized modulation cycles to achieve a favorable steady-state and transient performance.

A. Optimized Modulation Cycles

In conventional SVM, the reference voltage vector $\mathbf{u}_{s,\text{ref}}$ in one sampling interval T_s is approximated by a combination of two neighboring active voltage vectors \mathbf{u}_a , \mathbf{u}_b , and one zero vector \mathbf{u}_0 (or \mathbf{u}_7), see, Fig. 2. According to SVM, the application times of the voltage vectors can be calculated as

$$t_a \mathbf{u}_a + t_b \mathbf{u}_b = T_s \mathbf{u}_{s,\text{ref}} \quad (5)$$

$$t_o = T_s - t_a - t_b, \quad (6)$$

where t_a , t_b , t_o are the application times of \mathbf{u}_a , \mathbf{u}_b , and $\mathbf{u}_0/\mathbf{u}_7$, respectively. Note that t_o is divided into two equal time intervals located at the beginning and end of the modulation half-cycle to ensure that the harmonic current is zero when sampling occurs [15]. The impact of the voltage harmonics on the machine can be assessed by the harmonic model

$$\mathbf{v}_s = R_s \mathbf{i}_s + X_\sigma \frac{d\mathbf{i}_s}{dt}, \quad (7)$$

where $X_\sigma = \sigma X_s$, with $\sigma = (1 - \frac{X_m^2}{X_s X_r})$, is the total leakage reactance. The equivalent circuit representation of the harmonic model is shown in Fig. 3.

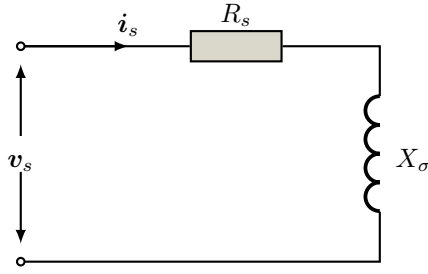


Fig. 3: Harmonic model of an induction machine.

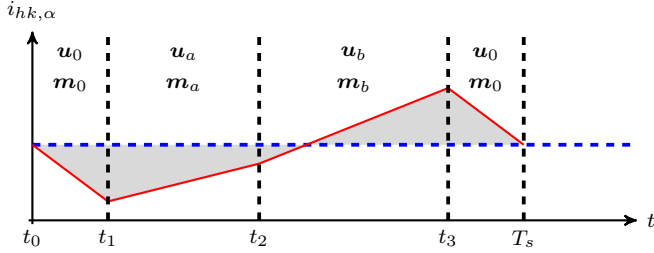


Fig. 4: The harmonic current (α -component) within one modulation cycle.

Based on Fig. 3, and by neglecting the stator resistance R_s , the harmonic current of an IM can be calculated as

$$i_{hk}(t) = \frac{1}{X_\sigma} \int_{t_0}^{t_0+T_s} (v_s(t, k) - v_{s,\text{ref}}(k)) dt, \quad (8)$$

where i_{hk} is the harmonic current of the k th modulation half-cycle, which starts at time instant t_0 , $v_s(t, k)$ is used to denote the voltage vectors within the k th modulation half-cycle, and $v_{s,\text{ref}}(k)$ is the sampled reference voltage vector.

Using the solution from SVM, and assuming the harmonic current is zero when the current is sampled, the evolution of the harmonic current i_{hk} within the k th modulation half-cycle can be calculated based on its gradients, i.e.,

$$i_{hk}(t) = \begin{cases} m_0 t & \text{if } 0 \leq t \leq t_1, \\ i_{hk}(t_1) + m_a(t - t_1) & \text{if } t_1 < t \leq t_2, \\ i_{hk}(t_2) + m_b(t - t_2) & \text{if } t_2 < t \leq t_3, \\ i_{hk}(t_3) + m_0(t - t_3) & \text{if } t_3 < t \leq T_s, \end{cases} \quad (9)$$

where

$$m_0 = -\frac{v_{s,\text{ref}}}{X_\sigma}, \quad (10a)$$

$$m_a = \frac{v_a - v_{s,\text{ref}}}{X_\sigma}, \quad (10b)$$

$$m_b = \frac{v_b - v_{s,\text{ref}}}{X_\sigma}, \quad (10c)$$

are the gradients of the harmonic current within the four subintervals, and $t_1 = \frac{t_0}{2}$, $t_2 = t_1 + t_a$ and $t_3 = t_2 + t_b$, as exemplified in Fig. 4.

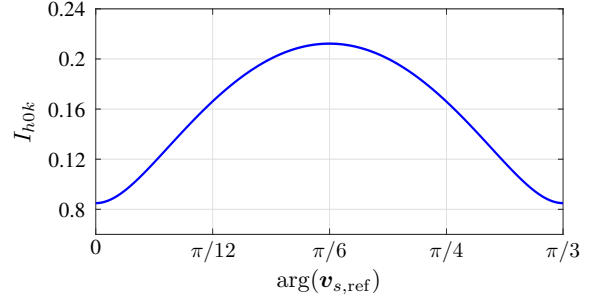


Fig. 5: The rms harmonic current in each modulation half-cycle I_{h0k} , when a fundamental period of $n = 42$ modulation half-cycles is considered. The modulation index is $m = 1.03$ and the total leakage inductance $X_\sigma = 0.11$ per unit (p.u.).

Based on (9), the rms harmonic current of the k th modulation half-cycle for a given reference voltage vector $v_{s,\text{ref}}(k)$ can be calculated as

$$I_{h0k} = \sqrt{\frac{1}{T_s} \int_{t_0}^{t_0+T_s} \|i_{hk}(t)\|_2^2 dt}. \quad (11)$$

When steady-state operation is considered, which means the amplitude of the reference voltage vector $v_{s,\text{ref}}(k)$ is constant, I_{h0k} is a function of the angle of $v_{s,\text{ref}}(k)$, see Fig. 5. As can be seen, when $v_{s,\text{ref}}(k)$ is close to one of the six active voltage vectors, the rms harmonic current I_{h0k} is relative smaller in the corresponding modulation half-cycles, while the opposite holds when $v_{s,\text{ref}}$ is in the middle of the sector.

Consider that the three-phase switching sequences are synchronized with the fundamental period. This means the fundamental period T_0 can be divided into an integer number n of sampling intervals

$$n = \frac{T_0}{T_s}. \quad (12)$$

The total harmonic distortion over a full fundamental period can be calculated as

$$I_h = \sqrt{\frac{1}{T_0} \sum_{k=1}^n I_{h0k}^2 T_s}. \quad (13)$$

Now we treat the sampling interval T_s as a variable T_k , while keeping the number of sampling intervals within one full fundamental period the same, i.e.,

$$\sum_{k=1}^n T_k = n T_s = T_0. \quad (14)$$

Similarly, the rms harmonic current I_{hk} of each time-varying sampling interval T_k can be calculated. By performing the same calculation as before, it can be obtained that

$$I_{hk}(\theta_k) = \frac{T_k}{T_s} I_{h0k}(\theta_k), \quad (15)$$

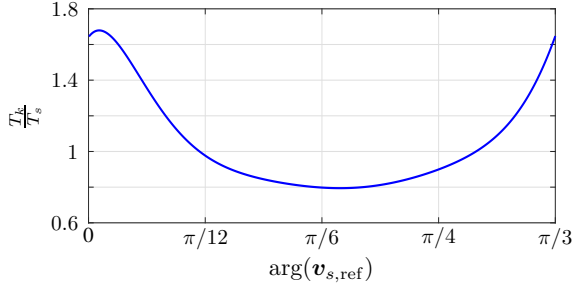


Fig. 6: The optimized modulation half-cycles T_k over one full fundamental period, with $n = 42$ and $m = 1.03$.

where θ_k is the angle of the reference voltage vector $\mathbf{v}_{s,\text{ref}}(k)$. As a result, the harmonic distortion within a fundamental period can be calculated as

$$I_h = \sqrt{\frac{1}{T_0} \sum_{k=1}^n I_{hk}^2 T_k} = \sqrt{\frac{1}{T_0 T_s^2} \sum_{k=1}^n I_{h0k}^2 T_k^3}. \quad (16)$$

Finally, the optimized sampling intervals T_k are obtained by solving the following optimization problem

$$\underset{\mathbf{T} \in \mathbb{R}^n}{\text{minimize}} \quad I_h \quad (17a)$$

$$\text{subject to} \quad \sum_{k=1}^n T_k = T_0 \quad (17b)$$

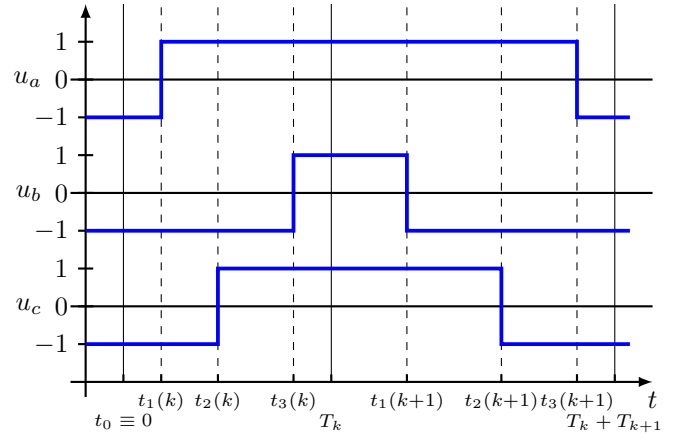
$$T_{s,\text{min}} \leq T_k \leq T_{s,\text{max}}, \forall k = 1, 2, \dots, n, \quad (17c)$$

where $\mathbf{T} = [T_1 \ T_2 \ \dots \ T_n]^T$, i.e., the vector of time-varying sampling intervals within one fundamental period, is the optimization variable. Regarding the constraints in (17), (17b) ensures that the number of sampling intervals over one fundamental period is fixed to n , thus guaranteeing that a fixed switching frequency results. Moreover, considering that a too short sampling interval may render the real-time implementation computationally infeasible, and a too long sampling interval deteriorates the sampling accuracy, the constraint (17c) limits the length of the optimized sampling intervals between a lower limit $T_{s,\text{min}}$ and an upper limit $T_{s,\text{max}}$.

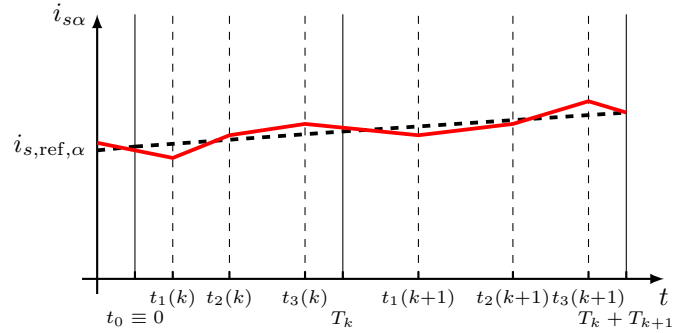
Fig. 6 shows one example of the optimized sampling intervals T_k over the interval $[0, \pi/3]$, while the function of T_k over the remaining five $\pi/3$ segments is identical due to symmetry. Note that the optimized modulation cycles T_k are independent from the machine parameters. They merely depend on the number of modulation half-cycles n and the modulation index m . Therefore, the optimized modulation half-cycles over one-sixth of the fundamental can be stored in a look-up table for different pairs $\{n, m\}$.

B. Optimal Control Scheme

The proposed control scheme combines the optimized modulation half-cycles with the direct MPC scheme in [10], [12]. At first, a steady-state operation with a fixed switching frequency is considered, which means the modulation index m and the number of modulation half-cycles n are constant. Then, the sampling interval T_k of each time step is decided



(a) Three-phase switch position.



(b) Stator current (α -component).

Fig. 7: Example of the evolution of $i_{s\alpha}$ over two sampling intervals by applying the depicted switching sequence.

by the angle of the reference voltage $\mathbf{v}_{s,\text{ref}}$, which can be obtained from the deadbeat solution $\mathbf{v}_{s,\text{db}}$. However, note that the deadbeat solution, in turn, requires the sampling interval T_k . Therefore, $\mathbf{v}_{s,\text{ref}}$ and T_k are approximated in an iterative manner. More specifically, let the initial guess $T_k^0 = T_s$, based on which the deadbeat solution $\mathbf{v}_{s,\text{db}}^0 \equiv \mathbf{v}_{s,\text{ref}}^0$ is calculated. Following, at the next iteration, T_k^1 can be obtained from $\arg(\mathbf{v}_{s,\text{db}}^0)$. By repeating this procedure, the required values are found and subsequently stored in a look-up table. Note that in practice, about two to three iterations suffice.

In the next step, the control problem is formulated as a constrained optimization problem, where the aim is to minimize the stator current ripple. To this aim, the gradients of the stator current are utilized. Moreover, in order to achieve a fixed switching frequency and an equal distribution of the switching power losses, each phase of the converter is allowed to switch once within the sampling intervals T_k , as exemplified in Fig. 7(a). More specifically, let t_z , $z \in \{1, 2, 3\}$, denote the switching time instants in chronological order within one sampling interval T_k , and $\mathbf{u}_{abc}(t_i)$, $i \in \{0, 1, 2, 3\}$, the switch positions in the four sub-intervals $[0, t_1)$, $[t_1, t_2)$, $[t_2, t_3)$ and $[t_3, T_k)$. Given that the sampling interval T_k is much smaller than the fundamental period T_0 , i.e., $T_k \ll T_0$, it is assumed that the stator current evolves linearly within each sub-interval.

TABLE I: Possible switching sequences for a two-step horizon.

Number of sequence	Phase with the switching transition					
	1 st sampling interval			2 nd sampling interval		
	First	Second	Third	First	Second	Third
1	a	b	c	c	b	a
2	a	c	b	b	c	a
3	b	a	c	c	a	b
4	b	c	a	a	c	b
5	c	a	b	b	a	c
6	c	b	a	a	b	c

Therefore, the stator current trajectories can be described by their corresponding gradients, i.e.,

$$\mathbf{m}(t_i) = \frac{d\mathbf{i}_s(t_i)}{dt} = \mathbf{C}(\mathbf{F}\mathbf{x}(t_0) + \mathbf{G}\mathbf{K}\mathbf{u}_{abc}(t_i)), \quad (18)$$

where $i \in \{0, 1, 2, 3\}$. Utilizing the gradients provided by (18), the stator current at the switching instants and discrete time steps can be calculated as

$$\mathbf{i}_s(t_i) = \mathbf{i}_s(t_{i-1}) + \mathbf{m}(t_{i-1})(t_i - t_{i-1}), \quad (19)$$

with $i \in \{1, 2, 3, 4\}$ and $t_4 = T_k$.

Note that by adopting the same principle, the current reference is assumed to evolve with a constant gradient within each sampling interval, given by

$$\mathbf{m}_{\text{ref}}(k) = \frac{\mathbf{i}_{s,\text{ref}}(k+1) - \mathbf{i}_{s,\text{ref}}(k)}{T_k}. \quad (20)$$

Hence, the current reference over the horizon is

$$\mathbf{i}_{s,\text{ref}}(t) = \mathbf{i}_{s,\text{ref}}(k) + \mathbf{m}_{\text{ref}}(k)t. \quad (21)$$

The above concept can be extended to longer prediction horizons to achieve better steady-state performance [16]. As shown in [12], by mirroring the switching sequences with respect to the discrete time steps the number of possible switching sequences is kept constant regardless of the prediction horizon steps N_p . In this work, a two-step horizon ($N_p = 2$) is implemented, as illustrated in Fig. 7. Table I summarizes all possible switching sequences over a two-step horizon.

Given the two-step horizon and the switching time instants and corresponding switch positions within each prediction step, the vector of switching time instants \mathbf{t} and the vector of switch positions (i.e., the switching sequence) \mathbf{U} are introduced, i.e.,

$$\mathbf{t} = [\mathbf{t}^T(k) \quad \mathbf{t}^T(k+1)]^T \quad (22a)$$

$$\mathbf{U} = [\mathbf{U}^T(k) \quad \mathbf{U}^T(k+1)]^T, \quad (22b)$$

where

$$\mathbf{t}(\ell) = [t_1(\ell) \quad t_2(\ell) \quad t_3(\ell)]^T \quad (23a)$$

$$\mathbf{U}(\ell) = [\mathbf{u}_{abc}^T(t_0(\ell)) \quad \mathbf{u}_{abc}^T(t_1(\ell)) \quad \mathbf{u}_{abc}^T(t_2(\ell)) \quad \mathbf{u}_{abc}^T(t_3(\ell))]^T, \quad (23b)$$

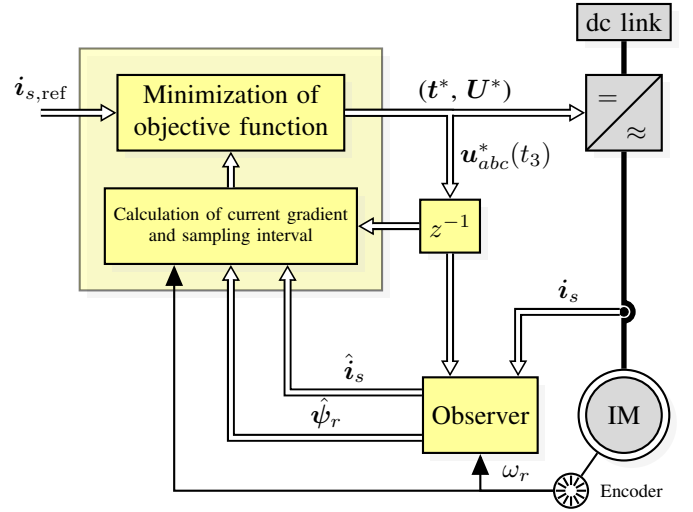


Fig. 8: Direct MPC with optimized sampling interval for a two-level three-phase voltage source inverter driving an IM.

Algorithm 1 Direct MPC with Optimized Sampling Interval

- Given $\mathbf{u}_{abc}(t_0^-)$, $\mathbf{i}_{s,\text{ref}}(t_0)$ and $\mathbf{x}(t_0)$
- 1: Compute iteratively the optimized modulation half-cycles, i.e., sampling intervals T_k
 - 2: Compute the corresponding gradient vectors \mathbf{m}_z , $z \in \{0, 1, \dots, 6\}$
 - 3: Enumerate the possible switching sequences \mathbf{U}_z , $z \in \{1, 2, \dots, 6\}$, based on $\mathbf{u}_{abc}(t_0^-)$
 - 4: For each \mathbf{U}_z , solve the QP (25). This yields \mathbf{t}_z and J_z .
 - 5: Find the minimum J_z . This yields \mathbf{t}^* and \mathbf{U}^* .
Return $\mathbf{t}^*(k)$ and $\mathbf{U}^*(k)$.

with $\ell \in \{k, k+1\}$ and

$$\mathbf{U}(k+1) = [\mathbf{u}_{abc}^T(t_3(k)) \quad \mathbf{u}_{abc}^T(t_2(k)) \quad \mathbf{u}_{abc}^T(t_1(k)) \quad \mathbf{u}_{abc}^T(t_0(k))]^T.$$

With all the above, the main control objective of (approximate) minimization of the rms stator current error is mapped into the objective function

$$J = \sum_{\ell=k}^{k+1} \left(\sum_{i=1}^3 \|\mathbf{i}_{s,\text{ref}}(t_i(\ell)) - \mathbf{i}_s(t_i(\ell))\|_2^2 + \|\mathbf{\Lambda}(\mathbf{i}_{s,\text{ref}}(T_\ell(\ell)) - \mathbf{i}_s(T_\ell(\ell)))\|_2^2 \right), \quad (24)$$

where the current tracking error is penalized at the switching time instants and at the discrete time steps. Moreover, the diagonal, positive definite matrix $\mathbf{\Lambda} \succ 0 \in \mathbb{R}^{2 \times 2}$ is introduced to penalize more heavily the tracking error at the discrete time steps [12, Section III].

After some algebraic manipulations, the control problem can

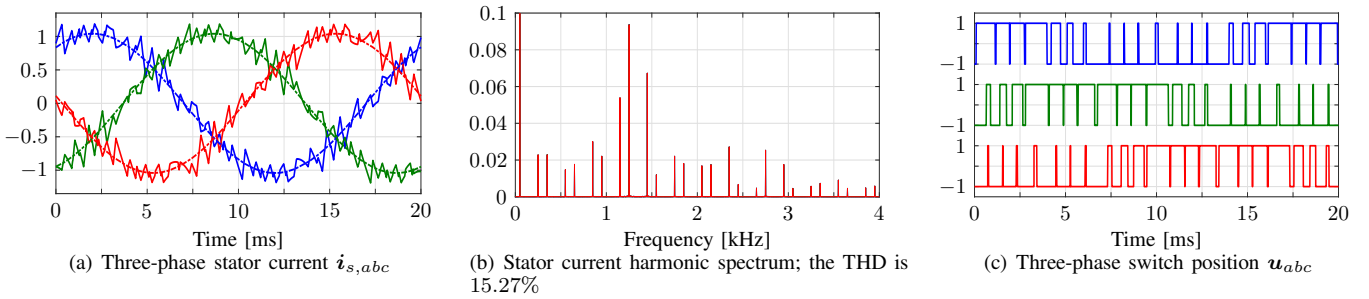


Fig. 9: Simulation results of direct MPC with optimized sampling intervals at steady-state operation, $f_{sw} = 1050$ Hz.

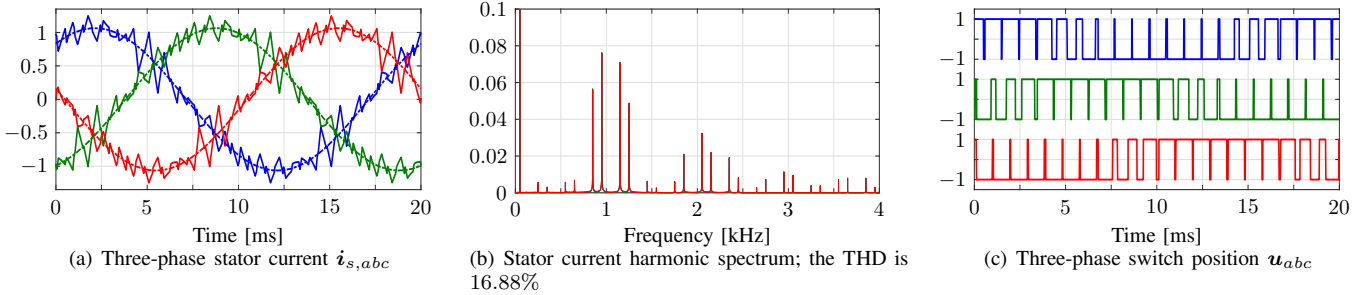


Fig. 10: Simulation results of FOC with conventional SVM at steady-state operation, $f_{sw} = 1050$ Hz.

be formulated as an optimization problem of the form

$$\begin{aligned}
 & \underset{\mathbf{t} \in \mathbb{R}^6}{\text{minimize}} && \|\mathbf{r} - \mathbf{M}\mathbf{t}\|_2^2 \\
 & \text{subject to} && 0 \leq t_1(k) \leq t_2(k) \leq t_3(k) \leq T_k \leq t_1(k+1) \\
 & && \leq t_2(k+1) \leq t_3(k+1) \leq T_k + T_{k+1},
 \end{aligned} \quad (25)$$

where the vector $\mathbf{r} \in \mathbb{R}^{8N_p}$ and matrix $\mathbf{M} \in \mathbb{R}^{8N_p \times 3N_p}$ can be found in [12].

To find the optimal switching time instants \mathbf{t}^* and corresponding optimal switching sequence \mathbf{U}^* , the QP (25) has to be solved six times, i.e., once for each possible switching sequence \mathbf{U}_z , $z \in \{1, 2, \dots, 6\}$, shown in Table I. The pair of switching sequence and time instants that is globally optimal, i.e., $\{\mathbf{U}^*, \mathbf{t}^*\}$, is chosen. In a last step, according to the receding horizon policy [3], only the switch positions that correspond to the first sampling interval are applied to the converter at the corresponding time instants. The block diagram of the proposed direct MPC scheme is shown in Fig. 8, and the pseudocode is provided in Algorithm 1.

IV. PERFORMANCE EVALUATION

This section presents the simulation results of the direct MPC scheme with optimized sampling intervals T_k . The examined system is a three-phase two-level voltage source inverter driving an IM (Fig. 1) with 380 V rated voltage, 5.73 A rated current, 3 kW rated power, 50 Hz nominal frequency and 0.11 per unit (p.u.) total leakage reactance. The inverter is supplied by a stiff dc source with the constant dc-link voltage $V_{dc} = 600$ V. The number of modulation half-cycles, i.e., sampling intervals, within one fundamental period was set to $n = 42$ so that a switching frequency of 1050 Hz results, assuming operation at rated speed. All results are shown in the p.u. system.

The steady-state performance of the direct MPC scheme is shown in Fig. 9. For comparison purposes, FOC with PI controllers and conventional SVM, i.e., with fixed sampling, was implemented, as shown in Fig. 10. As can be seen from Figs. 9(a) and 10(a), both controllers achieve accurate stator current tracking without any steady-state error. The resulting current harmonic spectra are shown in Figs. 9(b) and 10(b). FOC with SVM, due to its symmetric switching pattern and fixed switching frequency, produces discrete current harmonics concentrated only at the odd and non-triplen integer multiples of the fundamental frequency. As for the proposed direct MPC scheme, although the sampling intervals are no longer of fixed length, the symmetrical switching pattern is maintained, thus the harmonic energy is still concentrated at the odd and non-triplen integer multiples of the fundamental frequency. Moreover, the current THD with the direct MPC scheme is smaller, i.e., 15.27%, compared to that from FOC (16.88%). Finally, Figs. 9(c) and 10(c) show the three-phase switch position for direct MPC and FOC, respectively. It is observed that the direct MPC scheme with the optimized sampling intervals, similar to FOC, operates the converter at the constant switching frequency of 1050 Hz, despite the varying length of sampling intervals.

Finally, the transient performance of the two control schemes is shown in Figs. 11 and 12, where torque reference steps of magnitude 1 p.u. are imposed. As can be seen in Figs. 11(a) and 11(b), the direct MPC scheme, being a direct controller, achieves fast and accurate torque reference tracking during both the torque step-down and step-up transients. This happens even though the optimized sampling intervals are computed offline assuming steady-state operation. As for FOC, its dynamic response is much slower, as observed in Figs. 12(a) and 12(b). This is due to the smaller control bandwidth of the linear PI controllers.

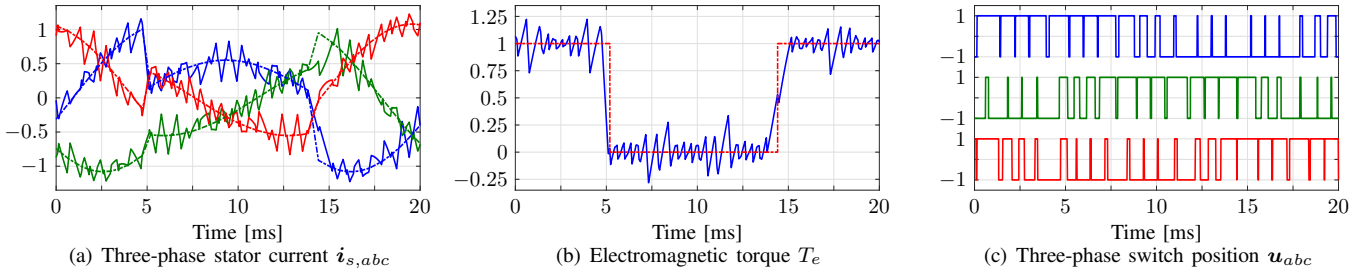


Fig. 11: Simulation results of direct MPC with optimized sampling intervals during torque reference step changes.

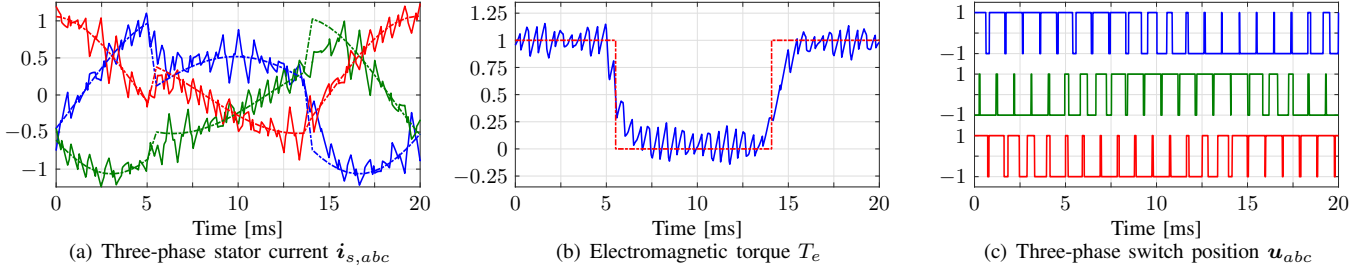


Fig. 12: Simulation results of FOC with conventional SVM during torque reference step changes.

V. CONCLUSIONS

In this paper we proposed a direct MPC scheme with optimized sampling intervals that achieves superior steady-state and transient performance. To achieve this, the sampling intervals that result in minimal current ripple are calculated offline in an optimal manner and are subsequently stored in a look-up table. Following, a direct MPC scheme is employed that utilizes the stator current gradients within a horizon of optimized time intervals, and aims for the minimization of the rms of the stator current ripple. As shown, by dropping artificial limitations that are imposed by the concept of a fixed modulation cycle, the direct MPC scheme can produce lower stator current THD and exhibit faster transient response, compared to FOC with conventional SVM.

REFERENCES

- [1] P. Cortés, M. P. Kazmierkowski, R. M. Kennel, D. E. Quevedo, and J. Rodríguez, "Predictive control in power electronics and drives," *IEEE Trans. Ind. Electron.*, vol. 55, no. 12, pp. 4312–4324, Dec. 2008.
- [2] P. Karamanakos, E. Liegmann, T. Geyer, and R. Kennel, "Model predictive control of power electronic systems: Methods, results, and challenges," *IEEE Open J. Ind. Appl.*, vol. 1, pp. 95–114, 2020.
- [3] T. Geyer, *Model predictive control of high power converters and industrial drives*. Hoboken, NJ: Wiley, 2016.
- [4] P. Karamanakos and T. Geyer, "Guidelines for the design of finite control set model predictive controllers," *IEEE Trans. Power Electron.*, vol. 35, no. 7, pp. 7434–7450, Jul. 2020.
- [5] J. Holtz, "Pulsewidth modulation for electronic power conversion," *Proc. IEEE*, vol. 82, no. 8, pp. 1194–1214, Aug. 1994.
- [6] L. Tarisciotti, P. Zanchetta, A. Watson, J. C. Clare, M. Degano, and S. Bifaretti, "Modulated model predictive control for a three-phase active rectifier," *IEEE Trans. Ind. Appl.*, vol. 51, no. 2, pp. 1610–1620, Mar./Apr. 2015.
- [7] S. Vazquez, A. Marquez, R. Aguilera, D. Quevedo, J. I. Leon, and L. G. Franquelo, "Predictive optimal switching sequence direct power control for grid-connected power converters," *IEEE Trans. Ind. Electron.*, vol. 62, no. 4, pp. 2010–2020, Apr. 2015.
- [8] L. Tarisciotti, A. Formentini, A. Gaeta, M. Degano, P. Zanchetta, R. Rabbeni, and M. Pucci, "Model predictive control for shunt active filters with fixed switching frequency," *IEEE Trans. Ind. Appl.*, vol. 53, no. 1, pp. 296–304, Jan./Feb. 2017.
- [9] L. Tarisciotti, J. Lei, A. Formentini, A. Trentin, P. Zanchetta, P. Wheeler, and M. Rivera, "Modulated predictive control for indirect matrix converter," *IEEE Trans. Ind. Appl.*, vol. 53, no. 5, pp. 4644–4654, Sep./Oct. 2017.
- [10] P. Karamanakos, R. Mattila, and T. Geyer, "Fixed switching frequency direct model predictive control based on output current gradients," in *Proc. IEEE Ind. Electron. Conf.*, Washington, D.C., USA, Oct. 2018, pp. 2329–2334.
- [11] A. Mora, R. Cárdenas-Dobson, R. P. Aguilera, A. Angulo, F. Donoso, and J. Rodríguez, "Computationally efficient cascaded optimal switching sequence MPC for grid-connected three-level NPC converters," *IEEE Trans. Power Electron.*, vol. 34, no. 12, pp. 12464–12475, Dec. 2019.
- [12] P. Karamanakos, M. Nahalparvari, and T. Geyer, "Fixed switching frequency direct model predictive control with continuous and discontinuous modulation for grid-tied converters with *LCL* filters," *IEEE Trans. Control Syst. Technol.*, vol. 29, no. 4, pp. 1503–1518, Jul. 2021.
- [13] J. Holtz and B. Beyer, "Optimal pulsewidth modulation for ac servos and low-cost industrial drives," *IEEE Trans. Ind. Appl.*, vol. 30, no. 4, pp. 1039–1047, Jul./Aug. 1994.
- [14] J. Holtz, "The representation of ac machine dynamics by complex signal flow graphs," *IEEE Trans. Ind. Electron.*, vol. 42, no. 3, pp. 263–271, Jun. 1995.
- [15] T. Matsui, T. Okuyama, J. Takahashi, T. Sukegawa, and K. Kamiyama, "A high accuracy current component detection method for fully digital, vector-controlled PWM VSI-fed AC drives," *IEEE Trans. Power Electron.*, vol. 5, no. 1, pp. 62–68, Jan. 1990.
- [16] T. Geyer, P. Karamanakos, and R. Kennel, "On the benefit of long-horizon direct model predictive control for drives with *LC* filters," in *Proc. IEEE Energy Convers. Congr. Expo.*, Pittsburgh, PA, USA, Sep. 2014, pp. 3520–3527.